

PHYSICAL REVIEW B

CONDENSED MATTER

THIRD SERIES, VOLUME 30, NUMBER 5

1 SEPTEMBER 1984

Further studies on the molecular dynamics of the glass transition and the glass state using EPR probes

Johanan Isaac Spielberg and Edward Gelerinter*

Physics Department and Liquid Crystal Institute, Kent State University, Kent, Ohio 44242

(Received 8 February 1984; revised manuscript received 15 May 1984)

Studies of an organic glass-forming liquid, dibutyl phthalate, with electron-spin-resonance probe molecules indicate a change in the primary relaxation mechanism about the glass transition. This is interpreted in terms of two different relaxation mechanisms of liquidlike and solidlike cells in the glass phase, as postulated in the work of Grest and Cohen. The observed gradual change of τ , the rotational diffusion time, above the glass-transition temperature is derived from the Grest-Cohen model. The sudden changes in line shape and signal intensity observed at the glass transition are interpreted in terms of EPR signal saturation effects and a possible abrupt change of T_1 , the spin-lattice relaxation time, due to the change of a substantial amount of the sample from the supercooled liquid state to the solidlike glass state. Spectral line simulations are used to verify phenomenological slow-tumbling τ formulas. The best fits to the experimental spectra at temperatures in the region of the glass transition are sums of simulated liquid and rigid EPR spectra. This provides evidence for the coexistence of two different types of regions from approximately 220 K and below.

I. INTRODUCTION

The subject of viscous flow in glass-forming liquids and the nature of the glass state has been the subject of many recent investigations.¹⁻³ In the high-temperature, low-viscosity regions of the liquid, viscosity and molecular-tumbling correlation times can be adequately matched using a classical activation-energy form for the viscosity,³

$$\eta = \eta_0 \exp(\Delta E/RT), \quad (1)$$

and the Stokes-Einstein relation⁴ for τ , the rotational correlation time,

$$\tau = 4\pi a^3 \eta / 3kT = A_0(\eta/T). \quad (2)$$

As the liquid is supercooled and the viscosity increases, the validity of both these equations may be questioned.³ A popular approach to the problem is the Vogel-Fulcher relation,^{5,6} which introduces a theoretical "ideal" glass-transition temperature T_0 ,

$$\eta = \eta_0'' \exp[B_0/(T - T_0)]. \quad (3)$$

Here, T_0 is usually 10–30 K below the observed glass transition. In 1951 Doolittle⁷ described a free-volume model which led to a relation

$$\eta = \eta_f \exp(\gamma V_0/V_f), \quad (4)$$

where γ is a constant near 1, V_0 is the van der Waals volume of the molecule, and $V_f = V - V_0$ is the free volume. Recently, Grest and Cohen^{1,8-10} published a new interpretation of the free-volume model that correctly fits the observed low-temperature supercooled-liquid η values, even in the region where η deviates from Arrhenius behavior. Previous free-volume calculations had the free volume $V_f \approx T - T_0$, whereas Grest and Cohen have

$$V_f \approx (T - T_g) + [(T - T_g)^2 + \beta T]^{1/2}, \quad (5)$$

and this V_f goes to zero only as T goes to 0 K.

This model has been shown to lead to a good fit of η versus $1/T$ for several glass-forming materials for η as high as 10^{14} P, and also leads to accurate T_g values when T_g is used as a matching parameter in τ -versus- $1/T$ fits via the Stokes-Einstein equation.^{11,12} The observed rotational correlation time τ , as calculated from EPR phenomenological formulas and line-shape matches, departs dramatically at lower temperatures from that value of τ predicted from any of the above η -versus- $1/T$ relations¹¹ and the Stokes-Einstein relation. In this region we observe a much lower activation energy which is at odds with the simple theory (see Fig. 1). It is one of the objectives of this paper to examine the nature of this variation of τ , and to give a theoretical justification for the observed values.

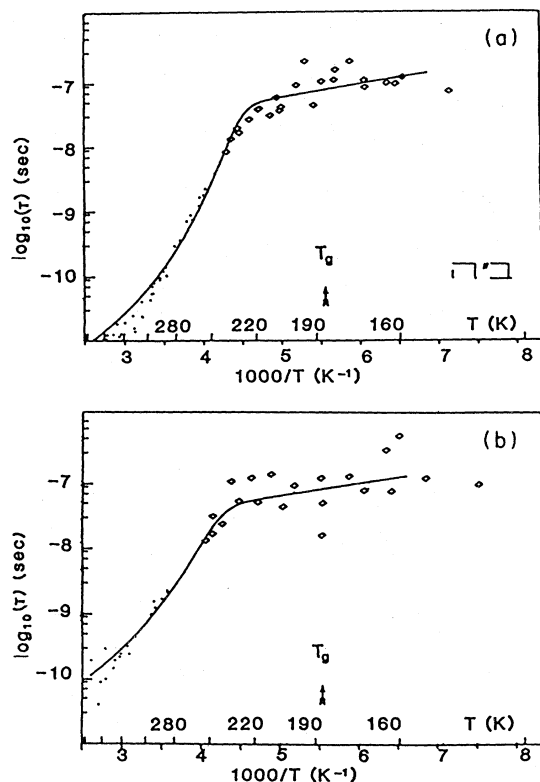


FIG. 1. Rotational correlation time τ is graphed as $\log \tau$ vs $1/T$ for (a) N-4 and (b) H-Tempone. The points are an average of τ_{iso} , τ_B , and τ_C for the high-temperature data and of phenomenological modes of Freed and Kuznetsov for the slow-tumbling regions. The curves are from Eq. (23) with the parameters (see Table III of Ref. 11) of the Grest-Cohen model and the activation-energy model used, respectively, for the high- and low-temperature relaxation sites of the model.

EPR spin-probe studies provide a powerful tool with which to observe the actual microscopic motions of probe molecules^{13,14} in the supercooled-liquid and glassy states. Although no abrupt changes of τ were observed upon passing through the glass transition, noticeable changes in spectral line shape and line height have been noted in the vicinity of T_g .¹¹ It is a second objective of this paper to further explore these changes and to interpret them in light of some of the various theories of the molecular nature of the glass state. A third objective of this research is to confirm the τ and EPR values obtained for different probes in the glass state using more sensitive techniques than were previously used.

II. THEORY

If one holds to a free-volume model of the supercooled liquid and glass, and considers the glass transition as defining a new type of "percolation problem," it is only natural to consider two types of sites in the glass phase, liquidlike and solidlike, which would each undergo different relaxational phenomena, characterizable with different relaxation times and activation energies. In addi-

tion, this would not be in contradiction with the model of the glass phase of liquidlike pockets caught in clathrate cages, as has been also suggested.^{7,15} Since the observed relaxation times and activation energies must be as a result of some combination of the liquidlike- and solidlike-cell motions, one would expect a deviation of observed values from the supercooled-liquid phase, where there are only liquidlike cells. Thus, one might expect some change in the system parameters as the glass state is approached; the exact nature and form of this change will be considered.

A. Glassy η and τ values

We wish to find a single relation that will predict the EPR observed rotational correlation time τ over the entire temperature range from low-viscosity liquid through the glass state. One might expect that such a relation must resemble one of the η viscosity formulas coupled with the Stokes-Einstein equation in the high-temperature region, and perhaps resemble to first order an activation-energy form for η coupled with some appropriate relation relating microviscosity to rotational relaxation in the low-temperature region. The joining of line-shape parameters reflecting disparate, simultaneously occurring physical processes has also been used in NMR studies to identify more than one ionization-level site.¹⁶ Many different studies have recently addressed the utility of modified Stokes-Einstein equations for molecular reorientation in liquids under varying experimental conditions.^{17,18} For this EPR problem, we propose to fit the entire temperature-viscosity spectrum with an equation of the form¹¹

$$1/\tau = 1/\tau_1 + 1/\tau_2 \quad (6)$$

Here, τ_1 may be related to the high-temperature liquid phase with the Stokes-Einstein relation and the Grest-Cohen model for η . In the low-temperature glass phase, the molecular-probe-tumbling time must reflect a local microviscosity. As it is derived in Debye's *Polar Molecules*,⁴ the Stokes-Einstein relation is valid for any relaxation from any small perturbation from an equilibrium rest state, and does not depend on the nonlocal parameters of the system. Therefore, this relation should be still useful for the glass state, even considering the nonhomogeneous nature predicted. One must calculate a proper average for the microviscosity, η_1 , measured in the glass phase in order to make use of this relation.

One may make use of the free-volume model and the Grest-Cohen formalism to do this (second equation numbers are from Ref. 1). They have the total translational-diffusion coefficient D defined as

$$D = D_0 p a_z(p) A_z(p) e^{-v_m/\bar{v}_f} \quad (7, 7.5)$$

Here, p is the fraction of liquidlike cells; if p is nonzero there are clusters of liquidlike cells, each of which has at least z liquidlike neighbors, if $p > p_c$ there is an infinite, connected liquidlike cluster, i.e., a liquid, and for $p < p_c$ there exists a glass. A measure of the liquidlike cells that belong to liquid clusters is given as $a_z(p)$, and $A_z(p)$ measures the number of clusters that are larger than some

minimum value v_m . The average free volume is \bar{v}_f . When v_m/\bar{v}_f is much less than the average cluster size \bar{v} , Eq. (7) may be rewritten as

$$D = D_0 p e^{-v_m/\bar{v}_f}, \quad (8, 7.6)$$

and one obtains the Doolittle equation. For liquidlike cells with volume $v \leq v_c$, \bar{v}_f does not adequately reflect the microfree volume and microviscosity of the local environment, as these parameters may be assumed to differ from the macrofree volume and macroviscosity of the glass as a whole. One may then solve for the microviscosity, for liquidlike-cell volumes, $v \leq v_c$.

One may derive the above results from an examination of the free-energy function of a cellular model of the glass or liquid. The local-free-energy function $f(v)$ contains two contributions, the negative of the work to remove a molecule from the interior of a cage of volume v , $f_0(v)$, and the work to expand the cage to the volume v from some suitable average value, $f_1(v)$ (see Fig. 2). The essential features of $f_0(v)$ are a minimum at v_0 and a point of inflection at v_1 . The discussion of $f_1(v)$ is more complex because it depends on the state of the neighborhood of the particular cell in question. For T near or above T_g , Grest and Cohen approximate $f(v)$ according to the following simple form:

$$f(v) = f_0 + \frac{1}{2}\kappa(v - v_0)^2 \quad \text{for } v < v_c, \quad (9, 3.4)$$

and

$$f(v) = f_0 + \frac{1}{2}\kappa(v_c - v_0)^2 + \zeta(v - v_c) \quad \text{for } v > v_c.$$

The parameters f_0 , $v_0 < v_c < v_1$, and ζ may be determined on a best-fit basis. From this equation one derives the free-volume model relation for viscosity η noted above, as well as relations correctly approximating the observed form of the entropy, heat capacity, and other parameters of the supercooled-liquid and glass phases, and the transition between them. This free-energy relation does not correctly predict the average free volume for the glass state, and one might try a first-order correction to the local-free-energy equation, for $v \leq v_c$, to solve for the microviscosity of the glass.

For the glassy state one imagines a local-free-energy function $f(v)$ that necessarily is composed of two parts: (1) For those cells that are solidlike (the $1-p$ solidlike cells) v is less than v_c and the first relation of Eq. (9) could be expected to hold,

$$f(v) = f_0 + \frac{1}{2}\kappa(v - v_0)^2 \quad \text{for } v < v_c, \quad (10, 3.4a)$$

and (2) for those cells that are liquidlike (p cells), v is greater than v_c and the second relation of Eq. (9) could be expected to hold,

$$f(v) = f_0 + \frac{1}{2}\kappa(v - v_0)^2 + \zeta(v - v_0) \quad \text{for } v > v_c. \quad (11, 3.4b)$$

For an average local-free-energy function, one alternatively might choose one of two approaches. We either let $f(v)$ equal $f(v)$ ($v < v_c$) and a term for $v > v_c$ proportional to the number of liquidlike cells,

$$f(v) = f_0 + \frac{1}{2}\kappa(v_c - v_0)^2 + p\zeta(v - v_c), \quad (12)$$

or let the local free energy be identical to that of the liquidlike state above T_g [Eq. (11)], and correct what final results one might obtain according to the consideration that only p of the cells have the additional term linear in $v - v_c$. Although the two approaches make different assumptions about where the averaging procedure of liquidlike and solidlike cells takes place, they both lead to the same result; this will be demonstrated.

Before continuing one must further consider the nature of $\zeta = \zeta_0 + \zeta_1$ for the p liquidlike cells of the glassy state. Above T_g this term has the form

$$\zeta(v - v_c) = \zeta_0(v - v_c) + \frac{kT_1}{v_a + \bar{v}_f}(v - v_c). \quad (13, 3.7, 3.8)$$

The first term of this expression increases monotonically with local free volume, while the second term should have a limit of about kT_1 for \bar{v}_f large, identifying $v - v_c$ with \bar{v}_f . In the other extreme for \bar{v}_f small, i.e., the glass state,

$$\zeta_1 \times (v - v_c) = \frac{kT_1}{v_a + \bar{v}_f}(v - v_c) \quad (14)$$

approaches another constant times a linear function of local free volume, $(kT_1/v_a)(v - v_c)$. This functional form

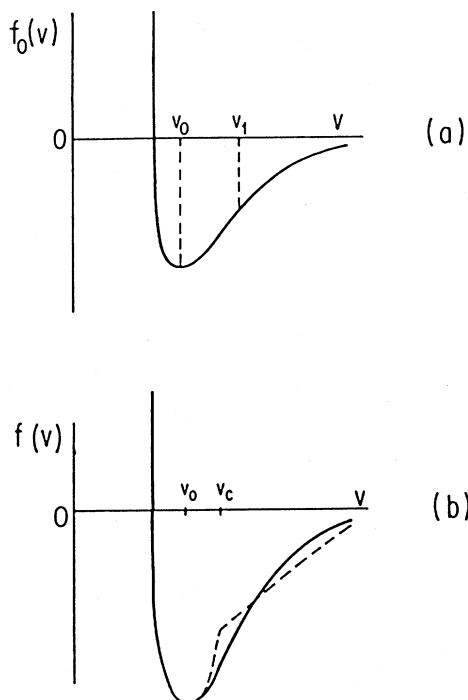


FIG. 2. (a) $f_0(v)$, the negative of the work to remove a molecule from the center of a cell vs cell volume v . The minimum of $f_0(v)$ is at v_0 , whereas v_1 marks the point of inflection. (b) Local free energy $f(v) = f_0(v) + f_1(v)$, where $f_1(v)$ is the work to expand the cage to the volume v from its average value. For $v < v_c$, $f(v)$ can be approximated as quadratic, and, for $v > v_c$, linear in its dependence on v , as shown by the dashed curve (Ref. 8).

should agree with one's intuitive view that the work required to expand the volume of given liquidlike cell might be linear in volume in the glassy state where presumably there are few (if any) neighboring liquidlike cells. One has for the glassy state ζ ,

$$\zeta_g = \zeta_0 + k \frac{T_1}{v_a} = k \frac{T_0}{v_a}, \quad (15)$$

where $kT_0 = kT_1 + v_a \zeta_0$, and \bar{v}_f is summed together with the fitted constant v_a . The change of $v - v_c$, the local free volume, compared to the change of \bar{v}_f in the glass, should be great, thus making it valid to consider \bar{v}_f as a constant for this purpose.

Using the first approach, we have

$$f(v) = f_0 + \frac{1}{2} \kappa (v_c - v_0)^2 + p \frac{kT_0}{v_a} (v - v_c). \quad (16)$$

Following the Grest-Cohen formalism, one may solve for the average free volume,

$$\bar{v}_f^{-1} = \frac{\zeta}{kT} - R_1, \quad (17, 6.12)$$

or, instead solving for the average free microvolume, we have

$$\bar{v}_{mf}^{-1} = \frac{pkT_0}{v_a kT} - R_1. \quad (18)$$

The term R_1 arises from including the communal entropy S_c in the calculation. The S_c in a liquid is due to the additional freedom each molecule possesses because it can diffuse throughout the entire volume, and is negligible in the glass phase at low temperatures. Letting $R_1 = 0$, as is also done in the calculation for macroviscosity,

$$\bar{v}_{mf} = \frac{Tv_a}{pT_0} = \frac{kT}{p(\zeta_0 + kT_1/v_a)}, \quad (19)$$

linear with T .

Using the second approach, one lets $\zeta = \zeta_g$ of Eq. (15), substitutes this value into the free-volume relation [Eq. (17)], and again lets $R_1 = 0$ to obtain

$$\bar{v}_f = \frac{kT}{\zeta_0 + kT_1/v_a} = \frac{kT}{kT_0/v_a} = \frac{v_a}{T_0} T, \quad (20)$$

again linear with temperature. Considering rotational diffusion only, the microviscosity could be expected to change as the free volume \bar{v}_f is localized to the liquidlike

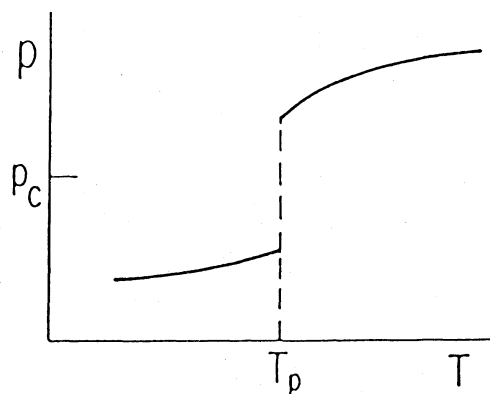


FIG. 3. Sketch of the probability of liquidlike cells p vs T near $T_p = T_g$ (Ref. 8).

cells,

$$\bar{v}_{mf} = \frac{1}{p} \bar{v}_f = \frac{kT}{p \zeta_g}, \quad (21)$$

the same relation as Eq. (19).

In order to calculate the rotational-diffusion relaxation time, one may determine a microdiffusion coefficient D_m from the diffusion equation (7) with \bar{v}_{mf} replacing \bar{v}_f , where \bar{v}_{mf} is the microfree volume defined above,

$$D_m = D_0 p a_z(p) A_z(p) e^{-v_m/\bar{v}_{mf}}. \quad (22)$$

For $v < v_c$, $a_z(p)$ and $A_z(p)$ can be expected to be less than 1, and p has the form shown in Fig. 3, a value close to unity above T_g , a value much smaller below T_g , and a sudden, discontinuous break at the glass-transition temperature. These equations are easily fitted to our EPR data. The activation energy ΔE is considerably smaller in the glass than in the liquid phase (say a factor of 3 to 10) as \bar{v}_{mf} would be expected to inversely increase with p . Similarly, $D_0 p a_z(p) A_z(p) (\eta_0)$ changes according to a scaling factor of form 10^3 to 10^5 over the same transition range. Part of this change may be accounted for from the change of value of p ; the rest perhaps comes from $a_z(p)$ and $A_z(p)$. These results may be used to roughly estimate the values of p and $a_z(p) A_z(p)$, as is done for our figures in Table I.

One may propose an all-temperature rotational-diffusion tumbling-time matching formula [Eq. (6)], using the Grest-Cohen η for the low-viscosity region, and $\eta_2 = D_m^{-1}$ [Eq. (22)] for the high-viscosity glass region,

TABLE I. Fitted results to Eqs. (1) and (2) for fast motional and supercooled liquid (l) and glass (g) regions. Ratios of the first columns are the source for the p and $pa(p)A(p)$ values in Eq. (7). The data of the first two results are from Ref. 11.

Probe	$A_l \eta$ (sec)	$\Delta E/R$ (K)	$A_g \eta$ (sec)	$\Delta E/R$ (K)	p	$pa(p)A(p)$
N-4	6.67×10^{-12}	3174	3.59×10^{-6}	261	0.082	1.9×10^{-6}
H-Tempone	8.5×10^{-15}	4403	2.56×10^{-6}	308	0.075	3.3×10^{-9}
N-4	1.0×10^{-14}	5146	3.37×10^{-6}	430	0.084	3.08×10^{-9}
D-Tempone	1.4×10^{-14}	4320	7.03×10^{-8}	851	0.197	2.04×10^{-7}

$$\begin{aligned} \tau^{-1} &= \left[\frac{4\pi a^3 \eta_0 \exp(-\gamma v_m / v_f)}{3kT} \right]^{-1} + \left[\frac{4\pi a^3 \eta_1 \exp(-\gamma v_m / v_{mf})}{3kT} \right]^{-1} \\ &= \left[\frac{\tau_{01}}{T} \exp \left[-\gamma \frac{v_m}{(T - T_g) + [(T - T_g)^2 + \beta T]^{1/2}} \right] \right]^{-1} + \left[\frac{\tau_{02} \exp(\Delta E / RT)}{T} \right]^{-1}. \end{aligned} \quad (23)$$

In both cases the Stokes-Einstein relation is used to convert from η to τ . One may argue that one is solely measuring the microviscosity of the p liquidlike cells, even in the glass, and so this relation is still valid. Equation (23) is fitted to the current data and previously reported data in Figs. 4 and 1, respectively.

Finally, one must address the question of the $1-p$ solidlike cells on the observed EPR spectrum. According to this model a large part of the molecules would be "frozen in" into an amorphous rigid structure near T_g . This would give rise to a characteristic amorphous powder pattern, as seems to be observed crudely at T_g . As the amorphous pattern might have very wide lines, and consequently be of low height, the peak positions [$H(\tau)$ and T_z ; see Fig. 6] noted and used for calculating τ in the slow-tumbling region¹¹ will still be those of the p

liquidlike cells that tumble faster, presenting narrower, taller lines. Our spectral simulations provide clear evidence for the coexistence of both types of spectra, thus strengthening the above interpretations.

B. Transition line heights and intensities: Saturation and T_1

From the Curie law one would expect the EPR signal intensity to be proportional to $1/T$, and one finds that this is indeed the case in the high-temperature region of the liquid. If the equilibrium spin population difference is disturbed, then the intensity of the EPR signal versus temperature will deviate from the $1/T$ dependence. One can show¹⁹ that

$$n = n^0 / (1 + 2PT_1). \quad (24)$$

In this equation, $n = n_l - n_u$ is the difference in population of the lower and upper energy levels, P is the stimulated-emission coefficient and is proportional to the radio-interaction magnetic field squared H_1^2 , T_1 is a relaxation time characteristic of the spin-lattice interaction, and n^0 is the thermal-equilibrium population difference. The interaction with the lattice restores the thermal-equilibrium populations, and makes possible the observance of any EPR signal. In normal, unsaturated conditions, PT_1 is much less than 1. If $2PT_1$ is comparable to or larger than 1, Eq. (24) describes the expected effect on the observed signal strength. These are known as saturation phenomena.

A simple relation¹⁹ for T_1 , where the only contribution to this value is from the tumbling of the molecules in a random field, $H(t)$, is

$$1/T_1 = (2g^2\beta^2/\hbar^2) \langle |H(t)|^2 \rangle \frac{\tau}{1 + \epsilon\omega_0^2\tau^2}, \quad (25)$$

where g is the average EPR Landé g factor, ω_0 is the spectrometer frequency, and ϵ is an experimental adjustment factor to account for shifts from Brownian diffusion of the nitroxide spin probe.²⁰ For an X -band spectrometer we have $\omega_0 = (2\pi \times 9.27 \times 10^9)$ rad/sec. For the cholestane probe, ϵ should have a value close to 1, whereas it has been found to be from 4–5 for the D- (deuterated-) Tempone probe. Equation (25) indicates that $1/T_1$ should increase roughly linearly with slower correlation time τ for τ much smaller than $1/\omega_0$. Larger values of τ would cause a decrease in $1/T_1$ or an increase of T_1 . As τ around the glass transition is often 2 or 3 orders of magnitude greater than this critical value, it is easy to see how saturation may occur.

Equation (25) was derived for a probe molecule in the liquid state, and cannot be expected to hold for relaxation in a solid crystalline or amorphous lattice.¹⁹ In a solid lattice more phonon-relaxation modes exist than in a liquid and T_1 should consequently have a smaller value.²¹

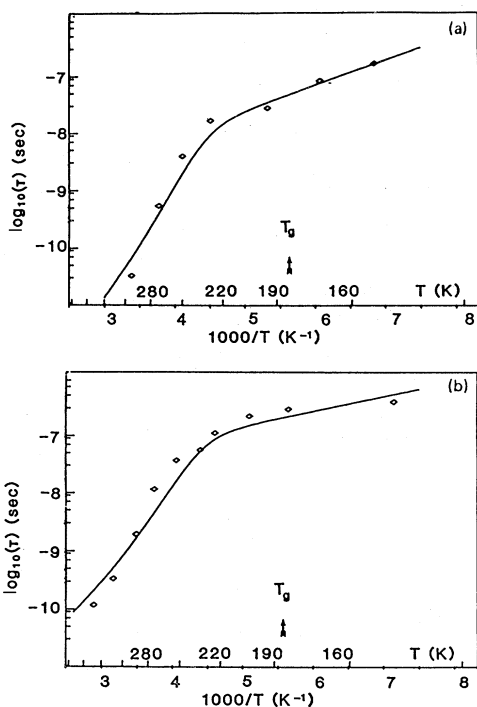


FIG. 4. $\log \tau$ vs $1/T$ is shown for (a) N-4 and (b) D-Tempone. The points are an average of τ_B and τ_C for the current data using the "best-fit" values of the Moro Lanczos algorithm program (Refs. 36 and 37). In the slow-tumbling regime, τ is the value used for the liquidlike component of the fitted composite spectrum. The curves are from Eq. (23), and the matching parameters used are, for (a), $\tau_{01} = 5.6 \times 10^{-10}$, $-\gamma v_m = 1908.0$, $T_g = 175.5$, $\beta = 58.4$, $\tau_{02} = 3.37 \times 10^{-6}$, and $\Delta E/R = 430$, and, for (b), $\tau_{01} = 6.1 \times 10^{-12}$, $-\gamma v_m = 2478.0$, $T_g = 184.5$, $\beta = 86.8$, $\tau_{02} = 7.03 \times 10^{-8}$, and $\Delta E/R = 851$.

A further test of the major liquidlike-solidlike transition at T_g , where $p = p_c$, may be found in an examination of the relaxation time T_1 . This transition may be found to show up indirectly as a change of signal intensities and line heights due to saturation effects.

C. EPR models, theoretical and phenomenological equations

Many different spin-resonance theories and models were used in this research, including fast and slow motional line-shape simulation programs, motional-narrowing theories, slow-tumbling phenomenological formulas, Heisenberg spin-exchange relations, and saturation $T_1 T_2$ formulas, to mention just a few. Rather than detailing all of the procedures here, essential details will be discussed as the results derived from them are called for in the paper.

III. EXPERIMENTAL TECHNIQUE

Two nitroxide spin probes were dissolved into separate samples of dibutyl phthalate, an isotropic organic liquid, and EPR spectra were observed from above room temperature to well below the reported²² transition temperature of $T_g = 175$ – 180 K. The glass-transition temperature was independently confirmed to have a value of 184.1 K using differential-scanning-calorimeter (DSC) techniques.²³ The samples were contained in quartz tubes (4 mm o.d., 3 mm i.d.). Spin label 611, obtained from Syva, Palo Alto, California 94304, is a large, cholesterol-shaped molecule with the nitroxide moiety replacing the hydroxyl group. One might expect this label to show Brownian-like motion due to its large size compared to the dibutyl phthalate molecule, and may also show considerable anisotropy in its tumbling characteristics because of its cigarlike shape. The chemical name is 4',4'-dimethylspiro(5 α -cholestane-3,2'-oxazolidin)-3'-yloxy, and it will hereafter be referred to as N-4. A 1-mM solution of N-4 in dibutyl phthalate was mixed in a test tube, lightly heated, and pipetted into a quartz tube. The sample was tested for a sufficiently intense EPR signal before being sealed. The second sample probe, 2,2,6,6-tetramethyl-4-oxopiperidinoxy, $C_6D_{16}NO_2$, commonly called deuterated (or D-) Tempone, was prepared at Kent State University, according to the method of Rozantsev.²⁴ The quartz sample tube was filled and tested in the same manner as for N-4. Before being sealed the sample was degassed using at least ten freeze-pump-thaw cycles to prevent oxygen broadening of the spectral lines.²⁵ The N-4 sample signal was compared with a degassed N-4 sample and no differences were detected, indicating that relatively little oxygen line broadening was present. D-Tempone is rela-

tively small and spherical in shape, and one expects that it would show almost isotropic tumbling characteristics and would diffuse according to a free-diffusion model. Because D-Tempone is deuterated, inhomogeneous line broadening should be minimized, thus simplifying computer line-shape simulations and also allowing for clearer observation of line-shape changes in the slow-tumbling supercooled-liquid and glass states. Electron-paramagnetic-resonance parameters for both probes are listed in Table II. These were obtained from computer simulations based on starting values obtained from literature sources.^{26–29}

To obtain the glass state, each sample was cooled within the spectrometer cavity at a rate estimated to be greater than 30 K/min. Measurements were made at increasing temperature, roughly every 10 K from 140 to 320 K.³⁰

The X-band paramagnetic resonance spectra were obtained using a modified Varian Associates model-4500 spectrometer. A Heath-Zenith model H-89 microcomputer was interfaced with the spectrometer to record magnetic field and derivative absorption values, and to control the magnetic field. This modification greatly improved general spectrometer performance and signal-to-noise values, and allowed digitization and storage of the spectra in a manner suitable for later analysis and simulation. The spectrometer-computer interface³¹ consisted of eight 12-bit multiplexed analog-to-digital converter (ADC) input ports, two of which were used for the spectrometer field and signal inputs, and four 12-bit digital-to-analog converter (DAC) ports, one of which was used to drive the external-field input on the Harvey-Wells magnetic power supply. Operational amplifier preamps were constructed for both of the input channels as well as a scalar for the field-drive output. The H-89 microcomputer 2-msec internal clock was used as the system timebase. Instantaneous display of the recorded signal was achieved through a serial output to a graphics-controller-operated 14-in. video monitor.

A modified Varian Associates model-4547 variable-temperature accessory was controlled with a temperature-controlling circuit built at Kent State University. The sample temperature was measured with a 36-gauge copper-constantan thermocouple inserted in the nitrogen stream that heated the sample. Over the entire temperature range the temperature variation was held to 0.2 K through the use of a copper and aluminum cane-shaped chimney on the outlet of the nitrogen cooling stream. The thermal gradient across the sample was estimated to be a maximum of 2 to 4 K in the lower temperature ranges.

Data analysis was done both on the H-89 microcomput-

TABLE II. EPR parameters were obtained from best fits of simulated lines to observed spectra. For both probes, $H_0 = 3330$ G, $\nu = 9.27$ GHz, $\omega_e = 2\pi\nu$, and $\omega_n = (8.8 \times 10^6)a_n$.

Spin probe	g_{xx}	g_{yy}	g_{zz}	A_{xx} (G)	A_{yy} (G)	A_{zz} (G)	a_n (G)	T_2 (G)
D-Tempone	2.0104	2.0074	2.0026	5.9	6.6	34.6	15.7	0.29±0.05
N-4	2.0090	2.0060	2.0020	6.8	6.0	34.8	15.9	1.10±0.15

er and larger main frame computers. Peak heights, B -field splittings, and area integrations were done with author-written Intel 8080 microprocessor assembly language programs on the H-89 microcomputer. Spectral line-shape simulations were made on a Burroughs B-6700 time-shared computer³²⁻³⁴ and a Digital Equipment Corporation VAX11/780 minicomputer using a UNIX operating system.³⁵⁻³⁷ PDP-11 family minicomputers were also used for some of the data analysis and curve fits found in this paper. Programs other than those separately referenced are either author-written or modified from published sources.³⁸

IV. RESULTS AND DISCUSSION

A. Line simulation, τ , and Heisenberg spin exchange

Rotational correlation times τ were calculated for all of the spectra gathered in a number of ways. For the purposes of calculating τ , it is convenient to view the EPR data as divided into two tumbling groups, fast and slow. The data of the fast-tumbling regime is adequately described by motional-narrowing theory,^{12,32-34} from which it is easy to calculate perpendicular, parallel, and average rotational correlation times τ . In the slow-tumbling regime, only recently have theoretical formulations representing τ been developed³⁹⁻⁴¹ to complement the phenomenological computer-simulation-based equations that have been previously employed,^{13,14,42-44} and these have not yet been widely used in EPR studies. In Fig. 1(a) we present data from previous research¹¹ of N-4 mixed with dibutyl phthalate. In the fast-tumbling regime τ_{iso} , τ_B , and τ_C were calculated based on the fast-motion-tumbling theory and averaged together. In the slow-tumbling region, τ was calculated according to phenomenological equations based on changes of some spectral features with τ , as determined from computer-simulated matches. Figure 1(b) is a similar plot of $\log\tau$ versus $1/T$ for H-Tempone (nondeuterated) with dibutyl phthalate. In the present research, detailed line-shape simulations were prepared in order to confirm the fast-motion and phenomenological equations and to provide a closer look at the nature of particularly the slow-tumbling regime of the supercooled liquid and glass.

Line simulations were made using parameters obtained from the methods mentioned in the preceding paragraph as starting values. In the fast-motion regime, where the individual hyperfine lines are easily resolved, the starting values were often found to be within 15% of the simulated "best" fit. In the fast-motion region, inhomogeneous broadening can be expected to play an important role in the observed line shapes, especially for the D-Tempone probe, and should be corrected for in order to obtain the most accurate results.^{20,34} This problem was avoided in this work through fitting the D-Tempone probe data only at lower temperatures where the effect is of less importance. Fits were made on the basis of visual comparison between the recorded experimental spectra and the computer-generated simulations and on the basis of minimizing a reduced χ value obtained from a comparison of 256 points of the two lines. In the slow-motion-

tumbling region there were often large-order-of-magnitude discrepancies between the phenomenological equations and "best"-fit simulations. Indeed, occasionally the observed EPR parameter [$H(\tau)$ and T_{zz} ; see Fig. 6] on which the phenomenological equation was based changed in a manner contrary to that expected from the change of temperature and viscosity. This, undoubtedly, may be at least partially attributed to lower signal-to-noise levels in the wider slow-tumbling spectra and the general poorer ability of the EPR spectrometer to record differences between slower motions. These results may also be seen as a consequence of the presence of more than one tumbling site near and through the onset of the glassy state. A plot of $\log\tau$ versus $1/T$ is shown for the values calculated from line simulations for N-4 in Fig. 4(a) and for D-Tempone in Fig. 4(b).

One of the fitting parameters found to be critical for accurate line-shape simulation, especially in the slow-tumbling regime, of the EPR Lanczos algorithm program,^{36,37} is the Heisenberg spin-exchange frequency ω_{SS} .^{13,45,46} This interaction is a result of bimolecular collisions of radicals during which time an exchange integral J' is present, and because of the Pauli principle, a term must be added to the spin Hamiltonian,

$$H_{SS} = J(t) \vec{S}_1 \cdot \vec{S}_2, \quad (26)$$

where $J = 2J'$ and J is dependent on time because of the relative motion of the radical pairs. The apparent effect is to cause an exchange of nuclear environment for the electron spins. The effective exchange frequency can be written as

$$\omega_{SS} = \tau_2^{-1} J^2 \frac{\tau_1^2}{1 + J^2 \tau_1^2}, \quad (27)$$

where τ_2 is the mean time between new bimolecular radical interactions, and τ_1 is the interaction lifetime. For simple Brownian diffusion one may approximate these two times as

$$\tau_2^{-1} = 4\pi dDN \quad \text{and} \quad \tau_1^{-1} = D/d\Delta r_J. \quad (28)$$

Here τ_2^{-1} depends on the "interaction distance" d , the linear-diffusion coefficient D , and the density of radicals N . The "interaction potential" $J(r)$ is nonzero and equal to J only in the range $d < r < d + \Delta r_J$. Cases of weak, intermediate, and strong exchange have been reported in the literature.⁴⁶

Writing the linear-diffusion coefficient D as

$$D = \frac{kT}{6\pi a \eta} = A' \frac{T}{\eta}, \quad (29)$$

one may find ω_{SS} [Eq. (27)] from the rotational-diffusion value using the Grest-Cohen model for η as

$$\omega_{SS} = \frac{B'\tau/A'}{(\tau/A')^2 + C'} - D', \quad (30)$$

where A' , B' , C' , and D' are fitted constants. We found that even at fast correlation times a residual ω_{SS} should be included to best-fit the experimental data, therefore necessitating the additional D' constant. One may match the

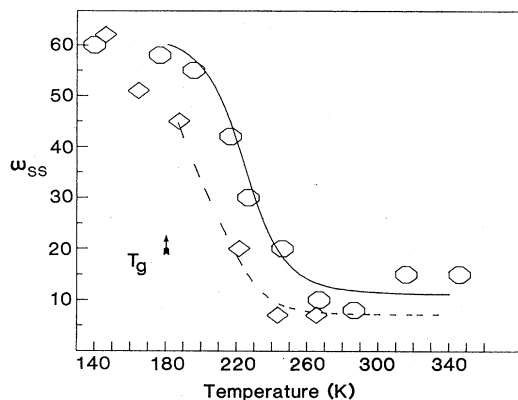


FIG. 5. Plotted here is ω_{SS} vs T for (a) N-4 and (b) D-Tempone. The curves are least-squares fits to the data of Eq. (30), with N-4 parameters of $A'=1.6$, $B'=2.0 \times 10^{-5}$, $C'=2.4 \times 10^{-4}$, and $D'=12.4$, and with D-Tempone parameters of $A'=6.9$, $B'=1.6 \times 10^{-6}$, $C'=4.9 \times 10^{-3}$, and $D'=11.0$.

ω_{SS} values used in the line simulations to this equation as has been done in Fig. 5. The shape of the curve and the corresponding matches are consistent with weak exchange, $J\tau \ll 1$. The flattening in the curves at low tem-

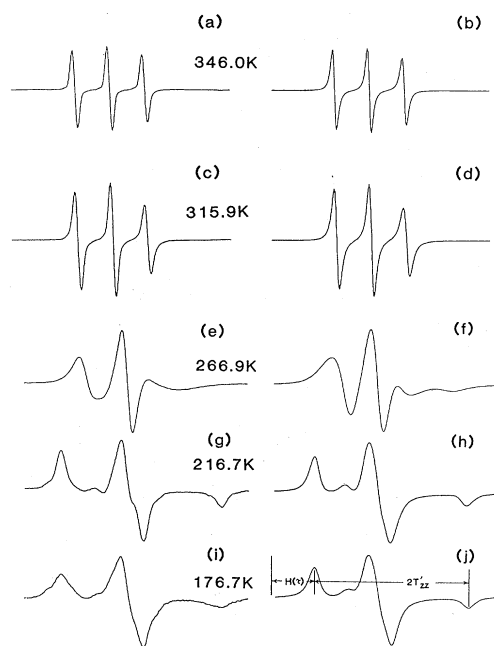


FIG. 6. (a), (c), (e), (g), and (i) N-4 experimental and (b), (d), (f), (h), and (j) theoretical "best-fit" spectra are plotted for different temperature samples. The Heisenberg spin-exchange frequency ω_{SS} used for each match is shown in Fig. 5, and the geometric mean of τ is shown in Fig. 4. The ratio of perpendicular to parallel diffusion constants, τ_{zz}/τ_{xy} , used varies from 1.5 to 2. In the slower-tumbling region the fitted spectra are actually sums of a "rigid-limit" spectrum, $\tau_{xy}=1.11 \times 10^{-6}$, $\tau_{zz}=1.67 \times 10^{-6}$, and $\omega_{SS}=80$ MHz, and a fast-tumbling spectrum, with values of τ that are plotted in Fig. 4. The rigid-limit spectrum comprises, respectively, 5% and 65% of the total spectrum in (h) and (j).

peratures follows the flattening of the observed τ values.

Representative fits of the N-4 data, which exhibit Brownian motion,⁴⁷ are shown in Fig. 6. The D-Tempone data, which exhibit intermediate jump diffusion, with a characteristic jump angle of 50° ,^{20,29} are shown in Fig. 7. The N-4 probe molecule, not being deuterated, is expected, due to the hydrogen hyperfine interactions, to exhibit more nearly Gaussian-shaped spectral lines, being narrower in the tail sections than Lorentzian spectral lines. This was found to be the case, and it affected our ability to match the tail regions of the experimental spectra. Still, the major features could be matched, and this is sufficient for τ estimates. The general spectral features of the simulation were found to be very sensitive to even small changes in some parameters and very insensitive to changes in other parameters. The spectral features are, of course, sensitive to τ and, as discussed above, to ω_{SS} . However, once $D_{xy}=1/(6\tau_{xy})$, the diffusion coefficient about the x - y plane, was fixed, the line shape was most insensitive to even large changes of $D_{zz}=1/(6\tau_{zz})$, the diffusion constant about the z axis. Thus, ratios of D_{xy}/D_{zz} are not necessarily exact, but only approximate indicators of the anisotropy of the tumbling. The N-4 and dibutyl phthalate experimental spectra were found to be better fitted at temperatures below 250 K with the Lanczos algo-

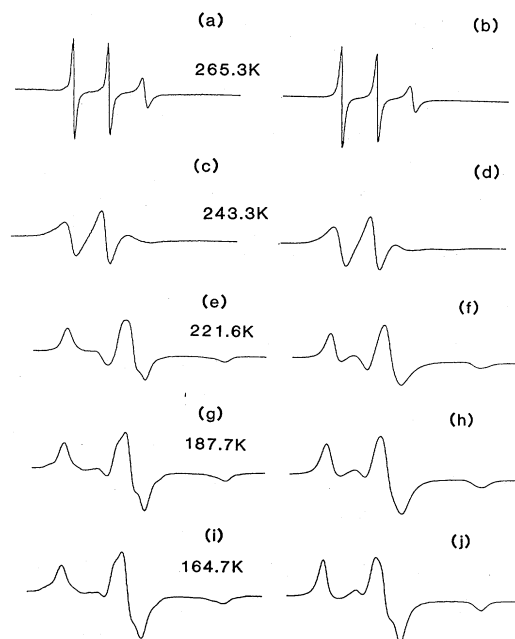


FIG. 7. (a), (c), (e), (g), and (i) D-Tempone experimental and (b), (d), (f), (h), and (j) theoretical "best-fit" spectra are plotted for different temperature samples. The Heisenberg spin-exchange frequency ω_{SS} used for each match is shown in Fig. 5, and the geometric mean of τ is shown in Fig. 4. As Tempone is known to tumble essentially isotropically, τ_{xy} was set equal to τ_{zz} for these fits (Ref. 11). In the slower-tumbling region, the fitted spectra are actually sums of a "rigid-limit" spectrum, $\tau_{xy}=\tau_{zz}=3.3 \times 10^{-5}$ and $\omega_{SS}=62$ MHz, and a fast-tumbling spectrum, with values of τ that are plotted in Fig. 4. The rigid-limit spectrum comprises, respectively, 10%, 25%, and 70% of the total spectrum in (f), (h), and (j).

rithm program that solves the full nonaxial EPR Hamiltonian. For the D-Tempone spectra and the higher-temperature N-4 spectra the algorithm neglecting all except the uniaxial terms and the nonaxial EPR simulation algorithm were found to match equally well the experimental spectra; thus the uniaxial program was used in these cases, even though the g tensor is not actually axial-symmetric.³⁷

B. Glassy spectral matches; slow-tumbling plus rigid-limit spectra

At temperatures well above the glass transition the probe may be thought to undergo nearly uniform relaxation and the observed spectra can be fitted with a single spectrum characterized by a single rotational-diffusion time. At lower temperatures, the spectra are best fitted with a linear combination of a slow-tumbling (large- τ) spectrum and a rigid-limit spectrum. The lowest-temperature spectrum that we observed for each probe, 139.8 K for N-4 and 154.0 K for D-Tempone, is taken as the rigid-limit spectrum. The rotational-diffusion time used for the liquidlike component of each match is based on starting values extrapolated from the phenomenological models previously described. At temperatures below the glass transition, the observed spectra are best-fitted with the 60–90% rigid-limit spectrum (depending on temperature) and the balance slow-tumbling spectrum. In this temperature region the dominant spectral shape is that of the rigid-limit spectrum. The general spectral shape would appear to be independent of temperature, but many of the spectral details would be influenced by the slow-tumbling spectrum which is still part of the composite spectrum. As the temperature is raised above the glass transition, the observed spectra are best matched using smaller percentages of the rigid-limit spectrum, with the relative percentages of liquidlike and solidlike spectra following approximately the form of Fig. 3, the graph of p , the percentage of liquidlike cells. Since the observed spectra appear to be sums of slow-tumbling and rigid-limit solidlike spectra, these observations provide support for the Grest-Cohen percolation model of the glass.

Another simple experimental demonstration of the two-tumbling-site model can be seen through a comparison of the recorded spectra immediately above and below the nominal glass transition. According to our model the spectrum just above the glass transition should reflect primarily liquidlike cells, whereas the spectrum just below the glass transition should reflect a primarily solidlike material. Subtracting a small percentage of the "liquidlike-above- T_g " spectrum from the "mostly-solidlike-below- T_g " spectrum should leave one with a spectrum reflecting almost only solidlike tumbling centers. This difference spectrum should be compared to a "rigid-limit" spectrum, where the lowest-temperature spectrum experimentally recorded may be used as an approximation to this theoretical limit. Figure 8 is our attempt at this procedure for the D-Tempone data. The two spectra plotted are the difference spectra, the highest-temperature glass spectrum (175.7 K) minus 15% of the lowest-temperature liquid spectrum (187.7 K), and

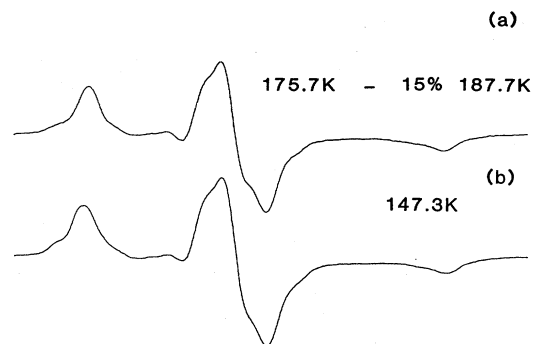


FIG. 8. How well one may approximate the glass phase as a mixture of liquidlike and solidlike cells is tested here, as (a) is the difference spectrum of a near-glass-transition-temperature glassy spectrum minus 15% of a near-glass-transition-temperature liquid spectrum, and (b) is the "rigid-limit" glassy spectrum presumed to have more solidlike and fewer liquidlike cells than the warmer glassy spectrum. The closeness of the match gives support to the two-site model.

our lowest-temperature rigid-limit spectra, at 147.3 K. The match is seen to be reasonable. Although the model used is probably an oversimplification of reality, it seems to adequately meet the test of practical utility in matching the experimental spectra and is theoretically plausible.

The spectra observed lower than 30–40 K above the glass transition may also be fitted through an increase in the average hyperfine-splitting tensor of approximately 1 G, instead of using a linear combination of spectra. Meirovitch *et al.*⁴⁸ observe a variation in the hyperfine splitting for the P probe in the liquid crystal pentylcyano-biphenyl (5CB) which they attribute to a distortion of the piperidine ring due to increased packing forces. The observed change in a_N was the order of 1 G for the flexible nitroxide probe used. Lee and Ames⁴⁹ report observing a change in a_N of a fraction of a gauss when observing the spectra from a more rigid probe dissolved in a polymer. Their probe has a shape similar to, but not exactly the same as, Tempone. Therefore we conclude that a small increase in the actual hyperfine tensor is possible, but its size is impossible to determine accurately. In addition, fitting the spectra only through changing a_N , leaves an additional problem, namely the unvarying nature of the spectra below T_g remains unexplained.

Therefore, we favor fitting the observed spectra in the thermal region from approximately 220 K to well below the glass temperature with linear combinations of rigid-limit and slow-tumbling spectra, and we feel that this result gives evidence favoring current glass theories.

C. Transition line shapes, line heights, spectral transforms, and line intensities

Although the measured τ rotational correlation time undergoes no sudden changes at T_g , there are a number of readily observable spectral line features that undergo pronounced changes at the glass-transition temperature. The spectral line shape takes on an essentially unchanging powder pattern form at T_g ,^{11,12} which is maintained ex-

cept for small changes at all recorded lower temperatures. This can be seen easily (Figs. 6–8) from plots of the lowest-temperature spectra scaled so as to all have the same overall height. At the same time that the spectral shape assumes an unchanging form, one finds a unique transition marker in the spectral line heights.^{11,12} For the cholestane probe, the central line height, which decreases remarkably from a high value, some 30–40 K above T_g , reverses its decline, and increases again, just below T_g . One finds the glass transition in a line-height valley, and one may compute an experimental T_g from the minimum of fitted cubic splines to these figures (Fig. 9). This effect was also seen with nondeuterated H-Tempone, as well as N-4 in earlier studies;^{11,12} however, the D-Tempone probe in our current work exhibits only a leveling of the peak-height decline without a subsequent increase.

In an attempt to explain the underlying phenomena behind these line-shape changes, we took Fourier transforms and performed power-spectrum analyses (auto-correlation functions) of all of our spectra.^{50–54} The Fourier transform of an EPR absorption signal is nominally just the magnetic susceptibility spectrum. In order to simplify the analysis of a spectrum, one may calculate the power spectral-density function as the sum of the squares of the real and imaginary parts of the transform, and use the spectral-density function as a window to view the underlying frequency, and hence linewidth, distribution of, in particular, the intermediate- and slow-tumbling spectra. In this way one may view the spectra as if one were observing random-noise spectra and pick out the underlying fundamental “transmitted”-frequency spectra. We used a Fortran-language fast-Fourier-transform program,⁵³ which, in reality, performs a finite Fourier transform on the input spectrum.⁵⁰ Typical power spectral-density functions are shown in Fig. 10. Peaks closer to the edges of the spectra of Fig. 10 represent higher-frequency components in the EPR spectra, thus reflecting narrower absorption or derivative lines, and are predominant in fast-motional, high-temperature spectra. Peaks closer to the center of spectra from Fig. 10 represent low-frequency components of the EPR spectra, reflecting wider lines, and are almost exclusively dom-

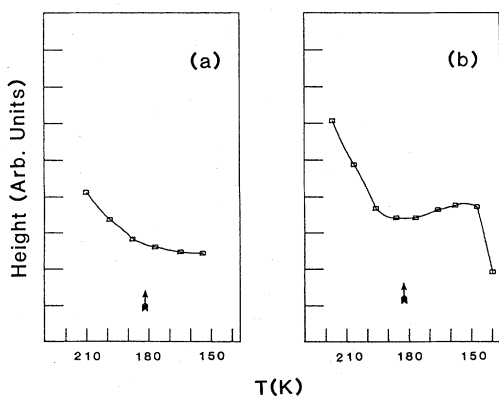


FIG. 9. Central-line height is plotted vs temperature for (a) D-Tempone and (b) N-4. The glass transition is indicated by the arrows. The cubic-spline-fitted line is drawn as a guide for the eye.

inant in slow-tumbling glassy and rigid-limit spectra. A tracing of the spectral Fourier frequency shifts from narrow-lined, high-temperature spectra, through the intermediate- to slow-tumbling regimes, and into the glassy rigid-limit region, is possible and does present valuable data that may otherwise be hidden from easy observation. Again, our interpretation of these spectra is limited to a comparison of power spectral-density line shapes as a function of temperature, to see what, if any, anomalies might be present in the various material states of the liquid or glass.

The frequency tracing discussed above is presented in Figs. 11 and 12. In Fig. 11 we plot, for N-4, a graph of spectral-density line height versus T , where each solid line corresponds to a different frequency channel of the spectral-density function. Each frequency channel is scaled in the graph to reflect the contribution of the channel to the area of the total spectrum, i.e., each channel is scaled proportionally to $1/f$. It is only necessary to graph half of the channels since the very high frequencies are a mirror image of the low frequencies (see Fig. 10). Figure 12 is the same plot for the D-Tempone and dibutyl phthalate data. Some expected and easily observed trends are noticed. First, the spectral distribution shifts from higher frequencies to lower frequencies, demonstrating that as T is decreased, η and τ are increased. This simply reflects the observation that a slower-tumbling probe molecule will produce a wider absorption peak. One should be able to identify the lines corresponding to the various interactions of the spin Hamiltonian and observe their changes with temperature. For example, the frequency

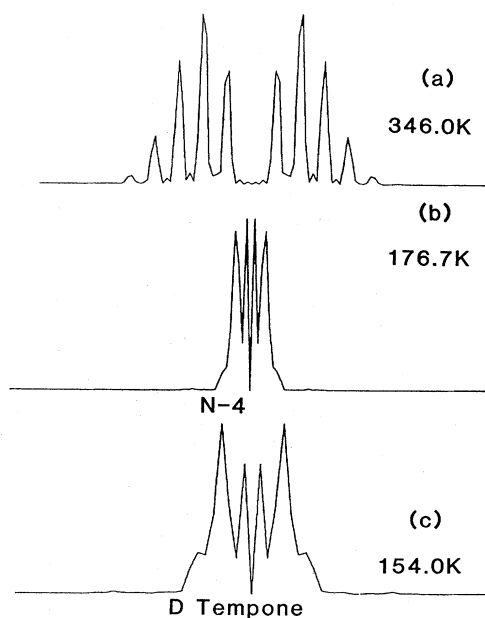


FIG. 10. Typical power spectral-density spectra [(a) and (b), N-4; (c), D-Tempone] are plotted, showing the shift from higher-frequency (outer lines) to lower-frequency components (inner lines) as temperature is lowered. The N-4 spectra show only the 64 lowest-frequency channels, while the D-Tempone spectrum shows only the 32 lowest. All of the spectra in the figure are scaled to be of uniform maximum height.

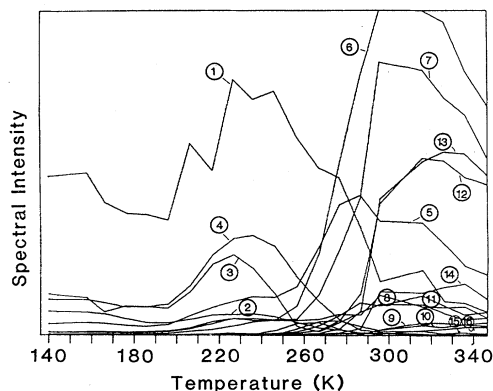


FIG. 11. For N-4, the intensity of the 16 lowest-frequency components of the derivative spectra measured using the power spectral-density function are plotted vs temperature. Since the lower-frequency components represent wider lines of lower intensity, each channel is scaled as $1/f$.

representing the average hyperfine splitting is seen to disappear roughly at the temperature at which one may no longer easily distinguish the individual spectral lines. This indicates the limit of the fast-motional analysis. Approaching the glass transition, one notices the setting in of a powder power-density spectrum, corresponding to the powder pattern observed in the derivative absorption signal. Lowered temperatures do not result in the elimination of additional lines from the frequency spectrum, but only in shifts of relative magnitude.

About the glass transition, along with this continuing shift from high-frequency narrow lines to low-frequency wide lines, one observes an additional result. There is a dip in the power spectra lines at all frequencies; every

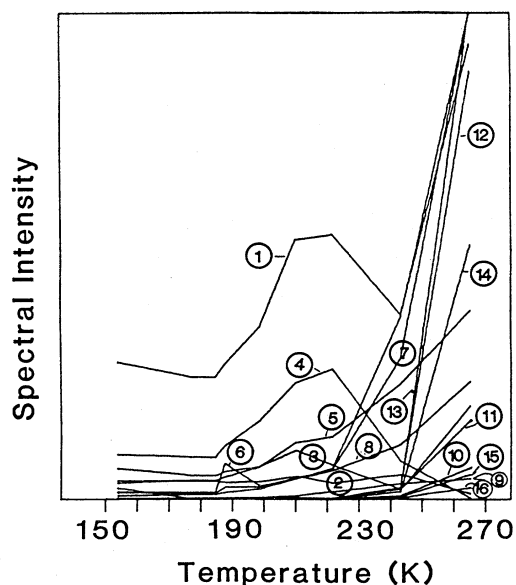


FIG. 12. For D-Tempone, the intensity of the 16 lowest-frequency components of the derivative spectra measured using the power spectral-density function are plotted vs temperature. Since the lower-frequency components represent wider lines of lower intensity, each channel is scaled as $1/f$.

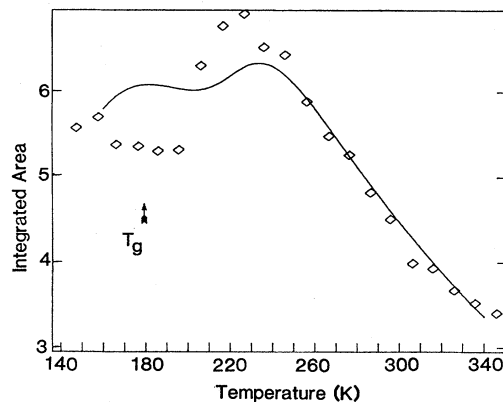


FIG. 13. Intensity of the absorbed microwave signal is plotted as the area under the integrated derivative spectrum in arbitrary units vs temperature for N-4. The curve is a least-squares best fit to Eq. (31) with $B_1=6629$, $B_2=6.3 \times 10^{-16}$, $\epsilon=1.0$, and a y -shift value of 18.3.

channel decreases as T goes towards T_g and increases sharply below T_g . This cannot be explained simply in terms of a shift of spectral signal from one frequency to another, as all of the channels decrease. Apparently there is a decrease in total signal intensity as the glass temperature is approached from above T_g , and an increase in total signal intensity just below the glass transition.

Figure 13 shows a plot of integrated intensity for the N-4 data, and Fig. 14 is the corresponding plot for the D-Tempone results. The integrated values were obtained from the derivative spectra using a Fortran-language program that iteratively solves for the proper zero baseline. One notices the increase in the intensity as the temperature is decreased in the high-temperature region. This is expected from the Curie law. Around 225 K, the signal intensity peaks and then begins to decrease. We attribute this to saturation phenomena. Recent measurements in our laboratory indicate that T_1 indeed increases rapidly between room temperature and 200 K.⁵⁵ One also sees a reversal of the signal-intensity decrease at the glass-

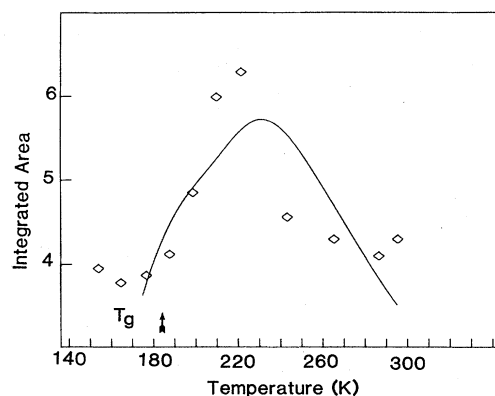


FIG. 14. Intensity of the absorbed microwave signal is plotted as the area under the integrated derivative spectrum in arbitrary units vs temperature for D-Tempone. The curve is a minimum-maximum best fit to Eq. (31) with $B_1=3258$, $B_2=8.96 \times 10^{-16}$, $\epsilon=4.24$, and a y -shift value of 7.52.

transition temperature T_g . The solid curve drawn fitted to the data is a least-squares fit to the Curie law, with the saturation result [Eq. (24)] substituted for N , the spin population difference, and the all-temperature rotational-diffusion relation derived above [Eq. (23)] used to calculate the rotational-diffusion correlation time τ . The final form of the fitting equation in our simple model is

$$I(T) = \frac{B_1/T}{1 + 2PT_1}, \quad (31)$$

where

$$2PT_1 = B_2 \frac{1 + \epsilon\omega^2\tau^2}{\tau},$$

with B_1 and B_2 as fitting constants, and an additional y-axis—shift value required to match the experimental results. With the observed scatter in the data, the fits do not appear to be very sensitive to the value of ϵ . Comparing Eqs. (31) to (25), one expects to find

$$B_2 = P \frac{2P\hbar^2}{g^2\beta^2 \langle |H(t)|^2 \rangle}, \quad (32)$$

where

$$P = c_\alpha^* c_\alpha = \gamma^2 H_1(t)^2 T_2. \quad (33)$$

In these equations the following definitions apply;^{19,25,56} the c_α are the eigenvalues of the transition matrix, $\gamma = g\beta/\hbar$, $H_1(t)$ is the peak value of the microwave magnetic field, and T_2 is related to the intrinsic linewidth of the derivative spectrum (Table II). One may estimate the value of H_1 from

$$H_1(t)^2 = (4Q_u P_c / \nu V_c) [1 + (C/nA)^2]^{-1} \quad (34)$$

in terms of the $Q_u \approx 2Q_L$ of the spectrometer cavity, the incident power of the cavity, P_c , the klystron frequency ν , the volume of the cavity V_c , a geometrical factor C/A equal to the cavity height divided into the cavity length and $n = 4$, for our TE₁₀₄ rectangular cavity. Furthermore, a correction factor of 2.5 times H_1 for the unperturbed cavity is included to account for the Dewar.²⁵ In calculating T_1 , one uses 72 MHz for a hyperfine-splitting anisotropy, as is observed for N-4 or D-Tempone,¹⁹ so that

$$(g^2\beta^2/\hbar^2) |H(t)|^2 = 4\pi^2 (72 \times 10^6)^2. \quad (35)$$

Thus, the lines of Figs. 13 and 14 correspond to the best-fitted curve of Eqs. (31) to the data above the glass temperature. The poorer fit in Fig. 14 may be partially a result of the large baseline errors introduced when one attempts to integrate narrow lines. Goldman *et al.*⁵⁷ have performed extensive saturation studies in the slow-motional regime. A motivation for these studies was the observation of differing line shapes in saturated and non-saturated spectra. We, however, do not observe appreciable differences in our N-4 data between the saturated and non-saturated spectra.

If the glass transition is taken to be the temperature at which an infinite liquidlike cluster forms, one may also interpret T_g , as a temperature denoting a substantial solidlike-liquidlike transition. The solid T_1 is highly

dependent on r_0 , the lattice separation,²¹ and the solid should, due to the increased number of phonon modes as compared to the liquid, be found to have a smaller value of T_1 . This would have the observed effect of bringing the EPR signal somewhat out of saturation as indicated through a jump in intensity. One finds the anomalous increase in intensity and line height at T_g to be a result of this liquidlike-to-solidlike-change-induced decrease of T_1 .

In order to experimentally verify this theoretical result, one may use saturation studies to determine T_1 directly above and below the glass transition. We have done this at three temperatures, and further, more complete and precise measurements are currently underway in our lab.

D. Saturation and T_1

A standard method to determine the transverse spin-lattice-relaxation time is through saturation studies.^{25,56,58} Following the discussion of Brezina and Gelerinter,⁵⁶ we find that the signal from the spectrometer with $\omega = \omega_0$ is given as

$$V_R = X/(1 + X^2), \quad (36)$$

with $X = \lambda H_1(T_1 T_2)^{1/2}$. The corner rf magnetic field $H_{1/2}$ is defined as that value of H_1 which makes $X = \frac{1}{2}$. This corner field can be determined from a plot similar to Fig. 15, which depends on the nature of the predominant broadening mechanism.^{56,58,59} Inhomogeneous broadening results from interactions independent of the spin system being studied, such as the hyperfine interaction, whereas spin diffusion gives more Lorentzian-shaped lines and results in homogeneous line broadening. The spin-spin-relaxation time T_2 can be estimated from the width of the homogeneously broadened line, and $T_1 T_2$ can be found from a saturation curve. Hence it is possible to determine T_1 for this simple case.

The experimental setup is the same as above. We calculated H_1^2 from Eq. (34), allowing for the impreciseness of our figures, and used the klystron attenuator to vary the incident power P_c without further testing of the calibration. This should give at least better than order-of-magnitude precision in the results. Finally, the peak-to-peak height of the central line was used as the indicator of signal intensity rather than the integrated absorption-spectrum intensity itself. This should not cause any trou-

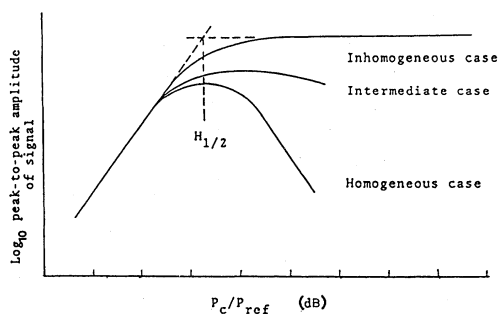


FIG. 15. Typical saturation curves showing the homogeneous, inhomogeneous, and intermediate saturation cases (Ref. 60).

ble, as spectra at differing klystron-attenuation levels, when scaled to the same maximum height were found to lie, within experimental error, one on top of the other, so that the line shape did not change appreciably with the varied power levels.

Figure 16 shows saturation curves for N-4 in dibutyl phthalate at room temperature, at 193 K (just above the expected glass transition), and at 162 K (just below the glass-transition temperature). A totally nonsaturated curve should show linear response of signal amplitude with increasing power. Figure 16(a), the room-temperature curve, most closely approximates these conditions, and the 10-dB amplitude value lies approximately on the nonsaturated line. Figure 16(b) shows substantial saturation even at 15 dB attenuation, while Fig. 16(c) shows no further increase in saturation, corresponding, we believe, to the solidlike onset of the glass transition. As all of our experimental spectra, except for those mentioned in this experiment, were obtained at 10 dB attenuation, Fig. 16(b) indicates that the supercooled spectra are clearly saturated. Our estimated and experimental results are presented in Table III. The spin-lattice-relaxation

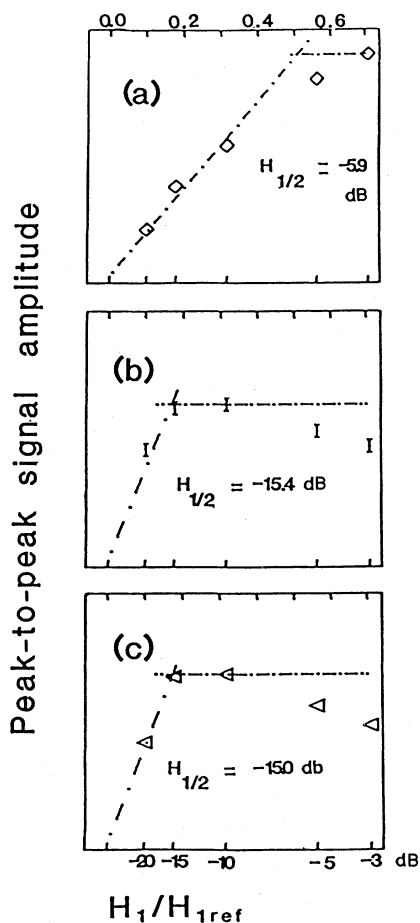


FIG. 16. Saturation curves are plotted for the N-4 probe at (a) room temperature (295 K), (b) above the glass transition (193 K), and (c) below the glass transition (162 K). Plotted is the central-line height vs $H_1/H_{1,ref}$, the root of P_c/P_{ref} in dB and as a decimal fraction.

TABLE III. Relaxation times obtained from saturation experiments. Spectrometer power output and Q_L were recently measured (Ref. 55), indicating a magnetic field incident on the sample at full power [Eq. (34)] to be $H_{1,0} \approx 0.345$ G. An invariant spin-spin-relaxation time of $T_2 = 3.59 \times 10^{-7}$ sec derived from spectral line simulations was used to find T_1 .

Temperature (K)	$H_{1/2}$ (dB)	$T_1 T_2$ (sec ²)	T_1 (sec)
295	-5.9	2.61×10^{-14}	7.27×10^{-8}
193	-15.4	2.33×10^{-13}	6.48×10^{-7}
162	-15.0	2.12×10^{-13}	5.91×10^{-7}

time T_1 can be seen to no longer increase in value at about T_g , presenting the possibility of some sort of phase change to account for the deviation from the simple theory for liquids. In the table, T_2 is determined from line-shape simulation using the methods discussed above, and the other calculations follow from Eqs. (34) and (36) and Fig. 16. We are repeating these measurements and extending them to the deuterated-Tempone probe over a wide temperature range. Preliminary room-temperature measurements indicate that D-Tempone saturates more easily than N-4.⁵⁵ When observed at room temperature at an attenuation setting of 10 dB, the signal from D-Tempone is already somewhat saturated. This is consistent with our observation of a relatively small region in Fig. 14 where the integrated areas increase with temperature.

V. SUMMARY AND CONCLUSIONS

A theoretical derivation of the reduction of the apparent activation energy for rotational diffusion, ΔE , from the classical low-viscosity result to the observed glass-state values, was presented based on the percentage of liquidlike cells in the material, p , following the formalism of the Grest-Cohen free-volume model of glass formation. This was shown to agree intuitively with a clathratelike-cage model of the glass and numerically with reported activation-energy figures.

We have extended our earlier^{11,12} EPR probe molecule studies of the liquid and glass states of some organic glass-forming liquids to include total line-shape determination of EPR and material parameters. This has led us to view the glass as a phase including two sites of different rotational correlation values, and the experimental EPR spectra as a sum of spectral components from each site. We also investigated the dependence of temperature and phase state on signal intensity and the power-frequency spectrum. The discovery of a pronounced signal-intensity variation at the glass transition led us to further investigate the dependence of temperature and state on the spin-lattice-relaxation time T_1 .

Additional conclusions, both theoretical and experimental, now are presented. (1) Inhomogeneous line broadening due to the hydrogen hyperfine interaction in N-4 substantially affects the recorded spectra. (2) The Heisenberg spin-exchange interaction follows the classical theory for both probes and is an important factor in the observed spectra, particularly at higher viscosities. (3) Cubic

splines fitted to the center-line peak heights versus temperature accurately predict the glass transition for the N-4 probe molecule. (4) The onset of the glass phase is also marked with a change to a rigid, almost unchanging, powder pattern, even with the narrow-lined D-Tempone probe. (5) This is interpreted as a result of a large percentage $(1-p)$ of the cells of the liquid becoming solidlike at T_g , leaving only p cells in a relatively fluid medium. (6) The measured τ of the glass is according to the model described above. (7) Power spectral analyses taken from Fourier transforms of the experimental spectra indicate shifts in the Hamiltonian linewidth components. These shifts can be plotted versus temperature, thus indicating the value of viewing the spectra in the spectral-density domain. (8) The setting in of the glass-state powder-pattern-like spectrum is also observed in the power-density spectra at T_g . (9) A dip in powder-density line heights at all frequencies just above the glass-transition temperature T_g indicates an anomaly other than the shifting of linewidth frequency components. (10) Measurement of total signal intensity unveils a $1/T$ Curie-law dependence in the low-viscosity region of the liquid, saturation phenomena in the supercooled liquid, and a reduction of the saturation effect in the glass state. (11) The measured intensities are fitted with least-squares-generated curves to the theoretically derived formula. (12) The reduction of the saturation effect is a result of a leveling of T_1 , the spin-lattice-relaxation time, brought about from the shift of a large fraction of the material from a

liquidlike to solidlike structure. (13) Saturation experiments with the N-4 probe confirm that the spectrometer signal is heavily saturated at the 10-dB attenuation level in the supercooled liquid. (14) The same experiments confirm leveling in T_1 below the glass-transition temperature. (15) One may therefore read the line-height and signal-intensity glass-transition indicators as a result of a combination of signal-saturation phenomena and the phase-dependent T_1 relaxation time.

The glass phase and the nature of its formation is still largely unexplored territory. Owing to the complexity and diversity of the yet unfolding structure, simple free-volume models and others still provide useful insights and directions for further research. Molecular-probe studies may be an important factor in the understanding of the microscopic organization and dynamics of glasses.

ACKNOWLEDGMENTS

The authors wish to thank Dr. Mary Neubert of the Liquid Crystal Institute (Kent, Ohio) for purifying and crystallizing the deuterated-Tempone spin probe, and Mr. David Chapman of Kent State University (Biology Department) for synthesizing this probe. The authors also wish to thank Dr. Norman V. Duffy of Kent State University (Department of Chemistry) for help in elucidating the structure and properties of the dibutyl phthalate molecule.

*To whom all correspondence should be addressed.

¹*Advances in Chemical Physics*, edited by I. Prigogine and S. A. Rice (Wiley, New York, 1981).

²J. Wong and C. A. Angell, *Glass Structure by Spectroscopy* (Dekker, New York, 1976).

³R. W. Douglas and B. Ellis, *Amorphous Materials* (Wiley, New York, 1972).

⁴P. Debye, *Polar Molecules* (Dover, New York, 1929).

⁵H. Vogel, *Z. Phys.* **22**, 645 (1921).

⁶G. S. Fulcher, *J. Am. Ceram. Soc.* **6**, 339 (1925).

⁷A. K. Doolittle, *J. Appl. Phys.* **22**, 1471 (1951).

⁸M. H. Cohen and G. S. Grest, *Phys. Rev. B* **20**, 107 (1979).

⁹G. S. Grest and M. H. Cohen, *Phys. Rev. B* **21**, 411 (1980).

¹⁰M. H. Cohen and G. S. Grest, *Phys. Rev. Lett.* **45**, 1271 (1980).

¹¹J. I. Spielberg and E. Gelerinter, *J. Chem. Phys.* **77**, 2159 (1982).

¹²J. I. Spielberg and E. Gelerinter, *Chem. Phys. Lett.* **92**, 184 (1982).

¹³P. L. Nordio and J. H. Freed, *Spin Labeling Theory and Applications* (Academic, New York, 1976).

¹⁴G. I. Likhtenstein, *Spin Labeling Methods in Molecular Biology* (Wiley, New York, 1974).

¹⁵M. H. Cohen and D. Turnbull, *J. Chem. Phys.* **31**, 1164 (1959).

¹⁶J. R. Hendrickson and P. J. Bray, *J. Magn. Reson.* **9**, 341 (1973).

¹⁷S. A. Zager and J. H. Freed, *J. Chem. Phys.* **77**, 3360 (1982).

¹⁸D. Kivelson and P. A. Madden, *Annu. Rev. Phys. Chem.* **31**, 523 (1980).

¹⁹N. M. Atherton, *Electron Spin Resonance* (Wiley, New York, 1973).

²⁰J. S. Hwang, R. P. Mason, L. P. Hwang, and J. H. Freed, *J. Phys. Chem.* **79**, 489 (1975).

²¹G. E. Pake, *Paramagnetic Resonance* (Benjamin, New York, 1962).

²²L. Ruby, B. J. Zabransky, and P. A. Flinn, *J. Phys. (Paris) Colloq.* **37**, C6-745 (1976).

²³J. S. Andrews (private communication).

²⁴E. G. Rozantsev, *Free Nitroxide Radicals* (Plenum, New York, 1970).

²⁵C. P. Poole, *Electron Spin Resonance* (Wiley, New York, 1983).

²⁶O. H. Griffith, D. W. Cornell, and H. M. McConnell, *J. Chem. Phys.* **43**, 2909 (1965).

²⁷W. L. Hubbell and H. M. McConnell, *J. Am. Chem. Soc.* **93**, 314 (1971).

²⁸J.-C. Hsia, H. Schneider, and I. C. P. Smith, *Can. J. Biochem.* **49**, 614 (1971).

²⁹S. A. Zager and J. H. Freed, *J. Chem. Phys.* **77**, 3344 (1982).

³⁰The authors wish to acknowledge Mr. Peter McCabe for taking the N-4 spectra.

³¹The authors wish to acknowledge Mr. Alan Baldwin for building the ADC-DAC interface and ARB-83 graphics controller.

³²C. F. Polnaszek and J. H. Freed, *J. Phys. Chem.* **79**, 2283 (1975).

³³J. H. Freed, G. V. Bruno, and C. F. Polnaszek, *J. Chem. Phys.* **75**, 3385 (1971).

³⁴S. A. Goldman, G. V. Bruno, C. F. Polnaszek, and J. H. Freed, *J. Chem. Phys.* **56**, 716 (1972). Programs courtesy of

- C. F. Polnaszek.
- ³⁵Computing Science Research Center, UNIX Time Sharing System, AT&T Bell Laboratories, Murray Hill, New Jersey, 07974 (1983).
- ³⁶G. Moro and J. H. Freed, *J. Phys. Chem.* **84**, 2837 (1980).
- ³⁷G. Moro, TRIDG, Cornell University Report, 1980 (unpublished). Programs courtesy of J. H. Freed.
- ³⁸W. N. Hubin, *Basic Programming for Scientists and Engineers* (Prentice-Hall, Englewood Cliffs, N.J., 1978).
- ³⁹S. Lee and D. Kivelson, *J. Chem. Phys.* **76**, 5746 (1982).
- ⁴⁰S. Lee, I. M. Brown, and D. P. Ames, *Bull. Am. Phys. Soc.* **27**, 191 (1982).
- ⁴¹A. Baram, *Mol. Phys.* **44**, 1009 (1981).
- ⁴²R. P. Mason and J. H. Freed, *J. Chem. Phys.* **78**, 1321 (1974).
- ⁴³A. N. Kuznetsov, A. M. Wasserman, A. U. Volkov, and N. N. Korst, *Chem. Phys. Lett.* **12**, 103 (1971).
- ⁴⁴R. C. McCalley, E. J. Schimshick, and M. H. McConnell, *Chem. Phys. Lett.* **13**, 115 (1972).
- ⁴⁵M. P. Eastman, R. G. Kooser, M. R. Das, and J. H. Freed, *J. Chem. Phys.* **51**, 2690 (1969).
- ⁴⁶M. P. Eastman, G. V. Bruno, and J. H. Freed, *J. Chem. Phys.* **52**, 2511 (1970).
- ⁴⁷K. V. S. Rao, C. F. Polnaszek, and J. H. Freed, *J. Phys. Chem.* **81**, 449 (1977).
- ⁴⁸E. Meirovitch, D. Ignier, E. Ignier, G. Moro, and J. H. Freed, *J. Chem. Phys.* **77**, 3915 (1977).
- ⁴⁹S. Lee and D. P. Ames, *Bull. Am. Phys. Soc.* **29**, 492 (1984).
- ⁵⁰Ron Bracewell, *The Fourier Transform and its Applications* (McGraw-Hill, New York, 1965).
- ⁵¹E. Oran Brigham, *The Fast Fourier Transform* (Prentice-Hall, Englewood Cliffs, N.J., 1974).
- ⁵²J. S. Bendat and A. G. Piersol, *Measurement and Analysis of Random Data* (Wiley, New York, 1966).
- ⁵³R. C. Singleton, *Commun. ACM* **10**, 647 (1967).
- ⁵⁴M. Rance, Ph.D. dissertation, University of Guelph, Ontario, Canada, 1981.
- ⁵⁵M. Plumley and E. Gelerinter (unpublished).
- ⁵⁶G. W. Brezina and E. Gelerinter, *J. Chem. Phys.* **49**, 3293 (1968).
- ⁵⁷S. A. Goldman, G. V. Bruno, and J. H. Freed, *J. Chem. Phys.* **59**, 3071 (1973).
- ⁵⁸B. Ford and E. Gelerinter, *J. Chem. Phys.* **55**, 3660 (1971).
- ⁵⁹A. M. Portis, *Phys. Rev.* **91**, 1071 (1953).
- ⁶⁰G. W. Brezina, Masters thesis, Kent State University, Kent, Ohio, 1968.